
# Phosphorus Sulfur/Graphene Composites as FlexibleLithium Sulfur Battery Cathodes with Super High Volumetric Capacity

Cheng-Chieh Chuang, Yi-Yen Hsieh, Wei-Chung Chang, Hsing-Yu Tuan

PII: S1385-8947(19)33319-4
DOI: https://doi.org/10.1016/j.cej.2019.123904
Reference: CEJ 123904

To appear in: *Chemical Engineering Journal*

Received Date: 10 September 2019
Revised Date: 18 December 2019
Accepted Date: 20 December 2019

Please cite this article as: C-C. Chuang, Y-Y. Hsieh, W-C. Chang, H-Y. Tuan, Phosphorus Sulfur/Graphene Composites as FlexibleLithium Sulfur Battery Cathodes with Super High Volumetric Capacity, *Chemical Engineering Journal* (2019), doi: https://doi.org/10.1016/j.cej.2019.123904

# Phosphorus-Sulfur/Graphene Composites as Flexible Lithium-Sulfur Battery Cathodes with Super High Volumetric Capacity

*Cheng-Chieh Chuang†, Yi-Yen Hsieh†, Wei-Chung Chang, and Hsing-Yu Tuan**

Department of Chemical Engineering, National Tsing Hua University, 101, Section 2, Kuang-Fu Road, Hsinchu, Taiwan 30013, ROC

*Email: hytuan@che.nthu.edu.tw

† These authors contributed equally to this work.

**ABSTRACT**

A phosphorus-sulfur/graphene composite (PS/G composites) cathode via a one-step PS additive reaction at 320°C is reported to achieve high volumetric capacities with a high sulfur packing density. The PS/G composites are self-supporting, bendable, and compressible, and can be easily compressed into a sheet of binder-free LiS cathode. The PS/G cathode with an extremely high cathode sulfur density of 1.8 g $cm^{-3}$ (active materials content of 80%) delivers an excellent specific capacity of 959 mA h $g^{-1}$, an areal capacity of 5.5 mA h $cm^{-2}$, and exhibits a low capacity fading rate (0.15% per cycle) within 200 cycles (~ 60% utilization). Consequently, the electrode gives a corresponding high volumetric capacity of 1726 mA h $cm^{-3}$ (the volume is based on all cathode materials plus current collector). Moreover, flexible devices of Li-S pouch cell using PS/G composites as cathodes shows stable electrochemical characteristics under bending condition, demonstrating their feasibility in commercial batteries.

**Keywords** lithium sulfur battery; volumetric capacity; phosphorus sulfide compound; high sulfur content; flexible

## Introduction

Li-S battery has a theoretical energy density of ~2600 Wh $kg^{-1}$,[1-3] much higher than the state-of-the-art Li-ion battery (~400 Wh $kg^{-1}$, practically achieved), and is considered as the next generation energy storage devices for light and durable portable electronic devices, long-driving-distance electro vehicles (EVs), and cheap massive grid energy storage.[4-5] S has been commonly studied as a cathode material due to its high theoretical capacity 1675 mA h $g^{-1}$, and is of high nature abundance, low cost, and nontoxicity.[6] However, the complex solid-liquid-solid mechanism has the following disadvantages:[7] (i) the low conductivity of sulfur and $Li_2S$ leads to poor utilization and dissolution of the intermediate polysulfide, resulting in a shuttle effect and fast performance degradation.[8-9] (ii) The volume change (80%) of S electrodes during the lithiation-delithiation process.[10-12] (iii) Large polarization and weak cycling stability with increased sulfur loading.

Various studies have been developed to address the mentioned problems by constraining S in a special cathode architecture,[13-21] capturing polysulfide through functionalized carbon materials[22-28], carbon-free sulfur immobilizer[29-30], intermediate layers[31-33]. In addition, designing different separators[34-35] and electrolyte system[36] is another way to deal with this major drawback to the Li-S cell. Most of these methods focus on confining polysulfides migration and withstanding volume expansion so as to improve the Coulombic efficiency. However, high-sulfur-loading electrodes made by conventional slurry coating routes are prone to cracking during processing and it is difficult to maintain their robustness due to

relatively large coating thickness,[37-38] furthermore, the ionic and electronic conductivity of electrodes are both reduced. Recently, electrodes of various engineered flexible architectures are designed for high energy density Li-S battery, such as core-shell,[39] carbon-cotton,[40] carbon nanotube paper,[41] carbon fiber foam,[42] 3D carbonaceous current collector,[43] and graphene or graphene oxide-based structure to realize high sulfur loading with high cathode integrity [44-46]Most studies firstly prepare the carbon support structure and then proceed with the sulfur insertion process. However, this route limits the cathode sulfur density of the electrode due to uneven filling and causes damage to the conducting network and flexibility of the electrodes upon further pressing. Meanwhile, the cathode sulfur density is relatively low, which leads to a bottleneck in the increase in volumetric capacity.

Electrodes with high sulfur loading can achieve the high energy density lithium sulfur battery. Recent developments highlight in areal mass loading and sulfur content, which are critical parameter to build the high energy LIS battery. To compete with the state of art Li-ion battery, the sulfur loading of 5 mg cm-2 is necessary. However, the high loading of sulfur increases the thickness of cathode and results in low volumetric capacity. In order to achieve high volumetric capacity, the cathode sulfur density is the point needed to be considered. In this study, we show a phosphor-sulfur (PS)/graphene(G) composite for use as a cathode of a Li-S battery. The PS/G composites have unique clay-liked characteristics that can be pressed into a flexible dense sheet so as to achieve an extremely high cathode sulfur density of 1.8 g $cm^{-3}$ (details of calculation and definition in Supporting information), resulting in a record high

volumetric capacity. The PS/G composites are prepared via a simple one-pot additive synthesis followed by mixing, heating and pressing procedures. Scheme 1 illustrates the preparation process of the PS/G composites cathode. PS/G black powders were prepared by mixing commercial red phosphorus, sulfur, and graphene. The sulfur containing powder is heated at 320 °C for 48 hr to increase the interaction between phosphorus and sulfur and graphene is also inserted during the synthesis. The PS structure percolated with grapheme is similar to arid clay, which can be easily pressed into sheets then cut to a suitable size. PS/G composites achieve a high volumetric capacity of 1726 mA h $cm^{-3}$ ($\rho = \frac{gram\ of\ sulfur\ in\ this\ cathode}{volume\ of\ all\ \ cathode\ materials\ plus\ current\ collector}$) with a high active material content of 80% and high sulfur loading of 6 ~ 10 mg $cm^{-2}$. Finally, the electrochemical performance of the flexible device of Li-S pouch battery made of PS cathodes were examined under a bending test.

**Results and discussion**

Phosphorus sulfide is obtained by heating red phosphorus and sulfur mixture above 300°C.[47-48] It is generally accepted that $P_4S_{10}$ convert to $P_2S_5$ with radical during heating reaction. Meanwhile, sulfur broken into short polysulfide chain with diradical end when heating above 250 °C.[49] After that, the short polysulfide chain then inserts into P-S-P bond of $P_2S_5$ to form P-$S_x$-P bond by additive reaction at 320°C.[50] Finally, PS compounds having a phosphorus to sulfur molar ratio of 1:20 was obtained. A typical photograph of the as-prepared PS compounds is shown in Fig. 1a. The PS compound is a deep green-yellow clay-liked material. The sheet with a small amount of cracks has good flexibility and can

be bent freely without damage. Fig. 1b-c shows the morphology of PS compounds imaged by scanning electron microscopy (SEM), revealing bulk and dense structures. After pressing, there are many cracks on the surface, indicating that the extensibility is limited. The chemical element mapping of P and S in Fig. 1d confirmed that PS compound has uniform distribution, indicating the additive reaction is completely. The PS compounds were investigated by X-ray photoelectron spectroscopy (XPS) to understand the surface species. P2p spectrum of XPS (Fig. 1e) is fitted and separated into two peaks at 131.9 and 133.3 eV, which correspond to the P−S bond.[50-51] Moreover, the fitting peaks found at 134.2 and 135 eV can be assigned to the phosphates[52] and $P_2O_5$.[50,53] Meanwhile, S2p spectrum of XPS (Fig. 1f) is separated into four peaks which is deconvoluted into contributions from S-S bond (163.5 and 164.7 eV), oxidized sulfur groups (168.4 eV),[54] and P-S bond (161.6 eV).[51] The surface of PS compounds is possibly oxidative while exposed to air or reaction environment. Furthermore, The $^{31}$P NMR spectra has been measured as shown in Fig. S3. The result confirms the molecular structure of the PS compounds, which is consistent with previous studies conducted by Qian et al.,[50] revealing four similar peaks providing the similar chemical environment of P in different PS compounds.

In order to practically use this self-supporting active material as a Li-S battery cathode, there have two issues need to be considered: (i) both phosphorus and sulfur have extremely low conductivity ($10^{-12}$ and $10^{-15}$ S $m^{-1}$) to impede electron transport. (ii) carbon additives must have great plasticity and withstand rolling compression. Graphene is a suitable candidate to address both issues due to its great electric

conductive and good solid lubricant[55], and it can also enhance the dipole-dipole interaction between lithium-polysulfide and cathode materials with π-electrons. A primary problem, however, is shuttle effect leading to the decreasing of capacity, shelf life and rate performances. Beyond the solution through strong lithium binding interaction between graphene and Li-polysulfide, another efficient approach is to employ an interlayer such as carbon paper inserted between separator and cathode.[56-58] Interestingly, in the analysis, the addition of graphene not only filled the crack and smoothed the surface, but also pressed the flakes, resulting in a higher cathode sulfur density,as shown in Fig.2a. The PS/G composites, exhibits self-supporting property and good flexibility. Fig. 1b-c and 2b-c clearly show that the PS/G composites has a smoother surface after pressing, indicating PS/G composites is more susceptible to compact compaction. Also, cross-section image presented the real thickness of PS/G composite shown in Fig. S10. Moreover, Fig. 2d shows the EDS mapping of PS/G composites, providing the nonhomogeneous distribution of phosphorus, sulfur and graphene. The reason may be attributed to two possible reasons: (1) PS compounds and graphene were forced to extend in different tension by the pressing process. (2) Although mixed by a ball milled process, the combination structure may have different models, such as encapsulated, wrapping or mixing, which results in uneven distribution of graphene. Furthermore, the P2p and S2p spectrum (Fig. 2e-f) of XPS of PS/G composites has the same main peaks as PS compounds, which present no further bonding in the additive reaction after adding graphene.

XRD patterns, TGA plots, and tensile tests of PS compounds and PS/G composites were shown in Fig.

3. The thermal gravimetric analysis (TGA) of PS/G composites shows a sharp weight loss between 250 °C and 300 °C under a nitrogen atmosphere, whereas PS compounds shows an irregular decline weight loss between 300 °C and 450 °C. The observed phenomenon of sublimation temperature depression may be resulted from the depth of additive reaction, which can be investigated in Fig. S4, further evidences little difference in P-S bonding.[59-61] Notably, the active material content of the PS/G composites remains at 80%, which guarantees the high energy density of the PS/G composites cathodes. In addition, the XRD patterns in Fig. 3b shows only the peaks of graphene (Fig. S2). Fig. 3c shows the mechanical properties of the PS compound and the PS/G composite measured by a tensile test, which display tensile strengths of 1 MPa and 4 MPa with Young's modulus of 117 and 688 MPa, respectively. Interestingly, the plastic deformation characteristic reveals PS compounds and PS/G composites both ductile properties. Meanwhile, the tensile strain of both is about 3.5%, which means that they can tolerate a certain degree of bending and stretching, and can be an ideal flexible material for Li-S battery.

The galvanostatic test of PS/G composites was performed in a CR2032 coin cell using lithium metal foil as the counter electrode operated in the range of 1.6 to 2.8 V. Fig 4a shows the PS/G composites had a discharge specific capacity 959 mA h $g^{-1}$ at 100 mA $g^{-1}$ after the first five cycles, and after 200 cycles, PS/G composites remained a specific charge capacity of 662 mA h $g^{-1}$, having the retention of 70% with respect to the specific charge capacity of the fifth cycle (959 mA h $g^{-1}$). Furthermore, the high density of PS/G composites give rises to an extremely high volumetric capacity of 1726 mA h $cm^{-3}$ and maintain a

capacity of 1321 mA h $cm^{-3}$ after 200 cycles. The slightly increase of capacity in the initial 20 cycles is the activation process of high loading Li-S battery. As the charge/discharge progress, this process guide the electrochemical reaction to a better kinetic position.[40, 62] Fig. 4b presents the corresponding voltage profiles of PS/G composites during cycling. It should be pointed out that the polarization of first cycle was very high, because of the high content of active material (80%) and the cathode sulfur density (1.75-1.88 g $cm^{-3}$, gram of active material per $cm^3$ of cathode volume) which retarded the efficient charge and ion transform pathway. The PS/G composites had a lithiation−delithiation specific capacity of 1685 to 692 mA h $g^{-1}$. The high irreversible capacity of in the first discharge−charge step results from the activation of the insulating active material, after cycling, the dissolved polysulfide migration accelerated the diffusing of active material to the conductive additive then finally stabilize the battery performance. In Fig. 4c, the rate capability is evaluated by changing current density from 0.1 A $g^{-1}$ to 3.36 A $g^{-1}$. PS/G composites display the specific discharge capacities of 1278, 1045, 972, 902, 785, 620 mA h $g^{-1}$ with corresponding volumetric capacity of 2193, 1791, 1670, 1560, 1354, 1062 mA h $cm^{-3}$, respectively. Moreover, when the current rate turns back to 0.17 A $g^{-1}$ after 55 cycles, the capacity of the PS/G composites can be recovered to 980 mA h $g^{-1}$ and 1682 mA h $cm^{-3}$. Fig 4d shows that the plateau of PS/G composites do not disappear with an increasing current density, indicating that the reaction still occurred at high current density. Fig. S5 depicts the comparative battery among the gravimetric capacity (mA h $g^{-1}$), areal capacity (mA h $cm^{-2}$), and volumetric capacity (mA h $cm^{-3}$) of different current densities for 200 cycles. The results indicate the great stability of the PS/G composites sulfur cathode, and we also

show SEM images, EDS mapping graphs and pictures of PS/G composites after cycling shown in Fig. S9. The results indicate the great stability of the PS/G composites sulfur cathode, and we also show SEM images, EDS mapping graphs and pictures of PS/G composites after cycling shown in Fig. S9. Fig. 5a shows the cyclic voltammetric (CV) containing 7 mg $cm^{-2}$ cathode at a scan rate of 0.1 mV $s^{-1}$, clearly indicating two redox pleatues appeared at 2.29 and 2.03 V. The higher potential is ascribed to the first lithiation process to form long-chain polysulfides and the lower potential corresponds to the further reduction of insoluble short-chain polysulfides.[10, 40, 63] For the anodic cycle, the pleatue appeared at 2.43 V, which revealed the oxidation process from precipitated $Li_2S/Li_2S_2$ back to sulfur.[40, 64] The up-shift of the redox peak and the down-shift of the oxide peak indicated the activating process within charge/discharge cycling. urthermore, the $Li^+$ diffusion coefficients ($D_{Li+}$) were evaluated by a series of CV curves with various scan rates and were calculated according to the Randles-Sevick equation. In the system of CVs shown in fig. S8, we assigned two cathodic peaks at around 2.3 V and 2.0 V and one anodic peak at around 2.5 V as peaks $C_1$, $C_2$ and $A_1$, respectively. The D values were determined to be D ($C_1$) = $6.58\times10^{-7}$ $cm^2$ $s^{-1}$, D ($C_2$) = $2.05\times10^{-7}$ $cm^2$ $s^{-1}$ and D ($A_1$) = $2.68\times10^{-6}$ $cm^2$ $s^{-1}$ for the coin cells (fig. S8 (b) ). Electrochemical impedance spectroscopy (EIS) test for cathode at charged-state are shown in Fig. 5b, measured in the range from 10 mHz to 10 kHz. The Nyquist plots illustrated a depressed semi-circle in the high frequency and a sloped line in the low frequency representing charge transfer resistance and Warburg diffusion process, respectively.[65-66] The uncycled cathode displays a high charge transfer resistance, however, after cycling, the results show a significant decrease in cell resistance, which

demonstrate the good electrolyte infiltration and fast charge transfer resistance within the activation process. The result also matches with the above mention of an activation process, the polysulfide migration helps the non-conducting active material diffusion. After achieving uniform distribution with conducting materials, that is, complete of activation process, the charge transfer might be stable at low position. Notably, the charge transfer resistance doesn't change after 20 and 50 cycles, which can describe the completed activation process.

The results in sulfur content, volumetric capacity and cathode sulfur density of PS/G composites with recent published high performance cathode are shown in fig. 6 (calculated values are shown in Table S1, Supporting information).[39-44, 66-71] In this comparison, the cathode sulfur density is estimated by gram of active material per cathode volume including current collector and all additive. In general, to increase sulfur content should create a carbon support with large space to put active materials, which result in low cathode sulfur density. Owing to PS/G composites' self-supporting property of both active and conductive materials with plasticity, it can be rolled into a sheet by high pressure pressing without the risk of structure damage. As a result, PS/G composites showed an ultra-high cathode sulfur density almost as high as 1.3 times the highest value reported by the top three in the active material content. In addition, the volumetric capacity of PS/G composites is the highest in the field. The PS/G composites offers great flexibility for extremely high cathode sulfur density and volumetric capacity through a pressure-sensitive design cathode.

As a proof of concept, the PS/G composites cathode and lithium metal are wound together with the separator and carbon paper to form a 0.5 cm × 5.3 cm and 0.7 cm × 5.5 cm pouch battery with thicknesses of 35 μm and 40 μm, respectively. To verify the practicality of the prepared flexible Li-S batteries, the pouch cell was first charge/discharge in the flat state shown in Fig. 7a. The PS/G composites pouch-cell at flat states delivered a discharge capacity of 18 mA h (Fig. 7a). We also demonstrate the pouch-cell start cycling at bending status that also can deliver a discharge capacity of 10 mA h under 167.5 mA $g^{-1}$ (Fig. S6). The pleatue appeared at 1.8-1.65 V may due to the lithiation of phosphorus oxide and the decomposition of $LiNO_3$ with complex reactions of intermediates in electrolyte. After the first four cycles, the side reaction disappeared and the platform returned to normal. Fig. 7b shows the stable voltage profile before and after the bending demonstration (Fig. 7c, and Movie S1 for the operation video). There is only slightly difference of capacity after the test. The inset is the cyclic performance, indicating stable Coulombic efficiency. Moreover, the PS/G composites battery is capable of illuminating up 40 LEDs in three different colors under various bending conditions (e.g., -180° to 180°) (Fig. 7c, Supplementary Movie 1). In the process of cylindrical bending and folding, the brightness of the LED does not change, which indicates the flexibility of the PS/G composite battery. Meanwhile, two Li-S pouch batteries in series can successfully illuminate four different colors of high voltage LEDs (Fig. 7d). Fig. 7e shows the tolerance of a flexible LIS battery under 5000 bends to Rc ~ 3.5 cm at a speed of 2 cm/s. The voltage stability of Li-S battery can be used to evaluate bending fatigue durability. During the continuous bending process, the cell voltage didn't change significantly. Only a small number of cycles

were observed a slight voltage jitter, which may due to the aluminum tab fracture, indicating that the PS/G composite pouch cell has good flexibility. Finally, Fig. 7f shows a photograph of the voltage retention test during a bending cycle where the tested Li-S battery is represented by two red dotted areas (see Movie S2 in the Supporting Information for the operation video).

In summary, a high density PS material is prepared by a one-pot additive reaction. This material has special clay properties and can be easily pressed into sheets and used directly as a sulfur cathode. To the best of our knowledge, the reported volumetric capacity and cathode sulfur density of PS/G composites in flexible sulfur cathodes have reached record highs. The excellent performance is attributed to the following reasons: First, graphene functions not only as an electronic conductive medium, but also as a lubricant for a pressing process to achieve high density. Second, PS compounds have good tensile and bending resistance, making them potential applications for flexible electronic devices. Based on the advantages of PS/G composites, the cathode delivers a high initial discharge capacity of 959 mA h $g^{-1}$ and an areal capacity of 5.3 mA h $cm^{-2}$ at 0.1 Ah $g^{-1}$ with a high sulfur load (6.5 mg $cm^{-2}$) and high active material content (~80%). Furthermore, the retention of PS/G composites at a charge and discharge rate of 0.17 Ah $g^{-1}$ still remained 70% after 200 cycles. The volumetric capacity of PS/G composites can reach 1726 mA h $cm^{-3}$, which is superior to other reports. In order to verify the practicability of the PS/G composite, a pouch cell was assembled and still exhibited stable performance under bending and folding. This study highlights the potential for the flexibility and high density as a cathode, providing superior

performance for Li-S cells and enabling PS/G composites to meet the requirements of the battery-powered market.

## Figures


**Scheme 1.** Schematic diagram of the process for fabricating PS/G composites materials.

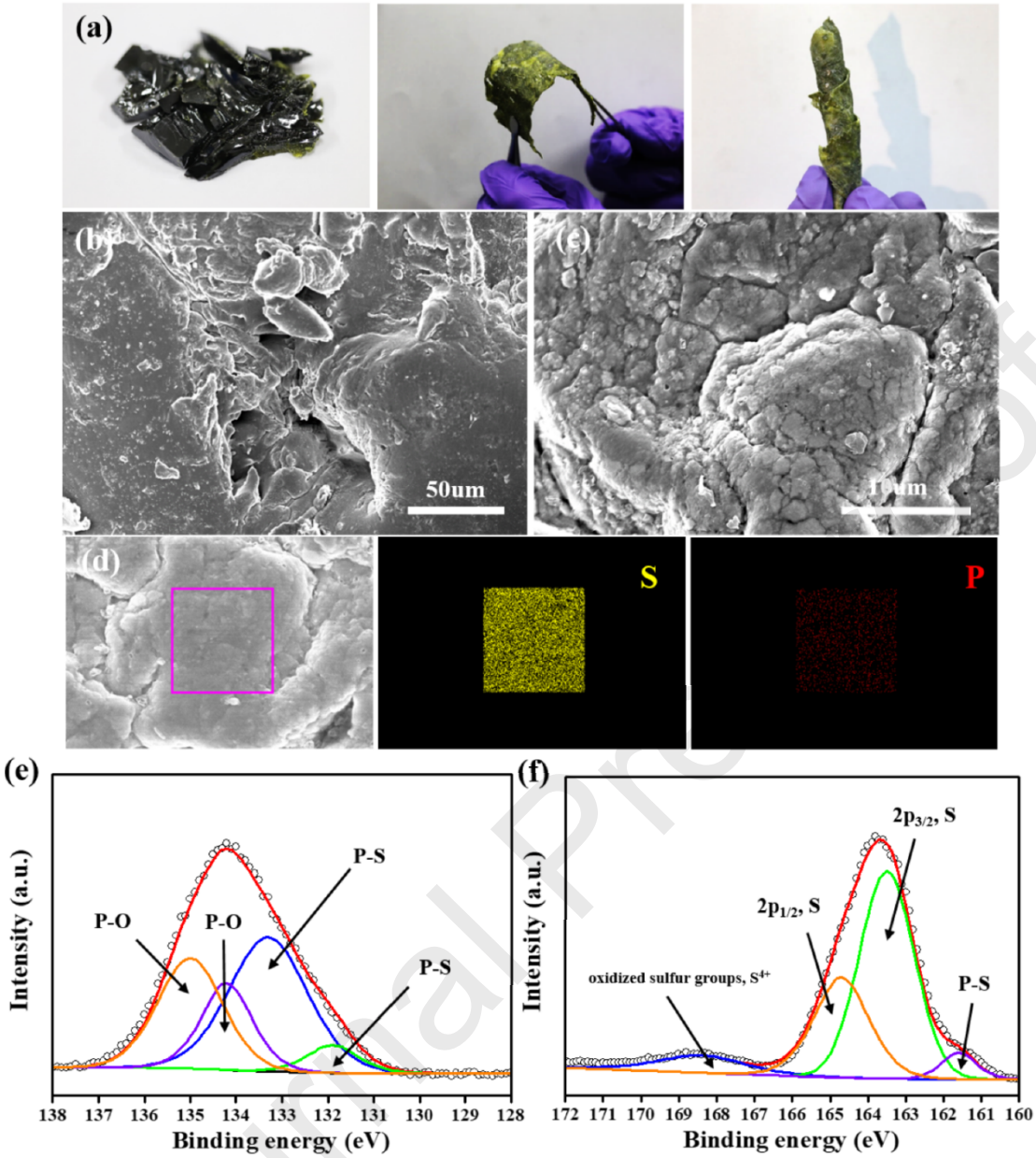


**Figure 1.** (a) Photograph of the PS compounds before and after pressing. SEM images of (b) before and (c) after pressing into sheet of PS compounds. (d) EDS elemental mappings of P (red) and S (yellow) of PS compounds. (e) P 2p and (f) S 2p XPS spectra and their fit curves for PS compounds.

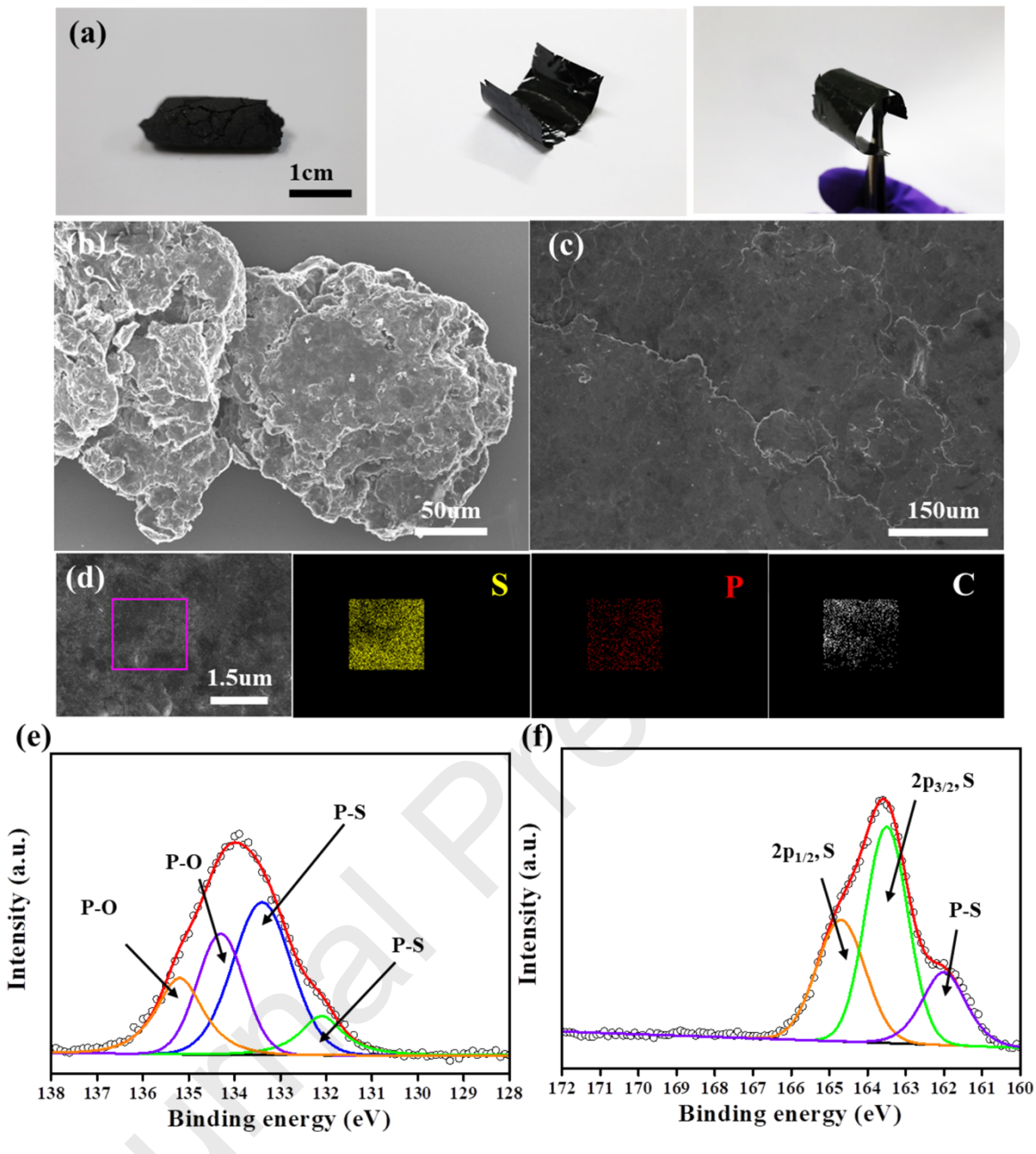


**Figure 2.** (a) Photograph of the PS/G composites before and after pressing. SEM images of (b) before and (c) after pressing into the sheets of PS/G composites. (d) EDS elemental mappings of P (red), S (yellow) and C (white) of PS/G composites. (e) P 2p and (f) S 2p XPS spectra and their fit curves for PS/G composites.

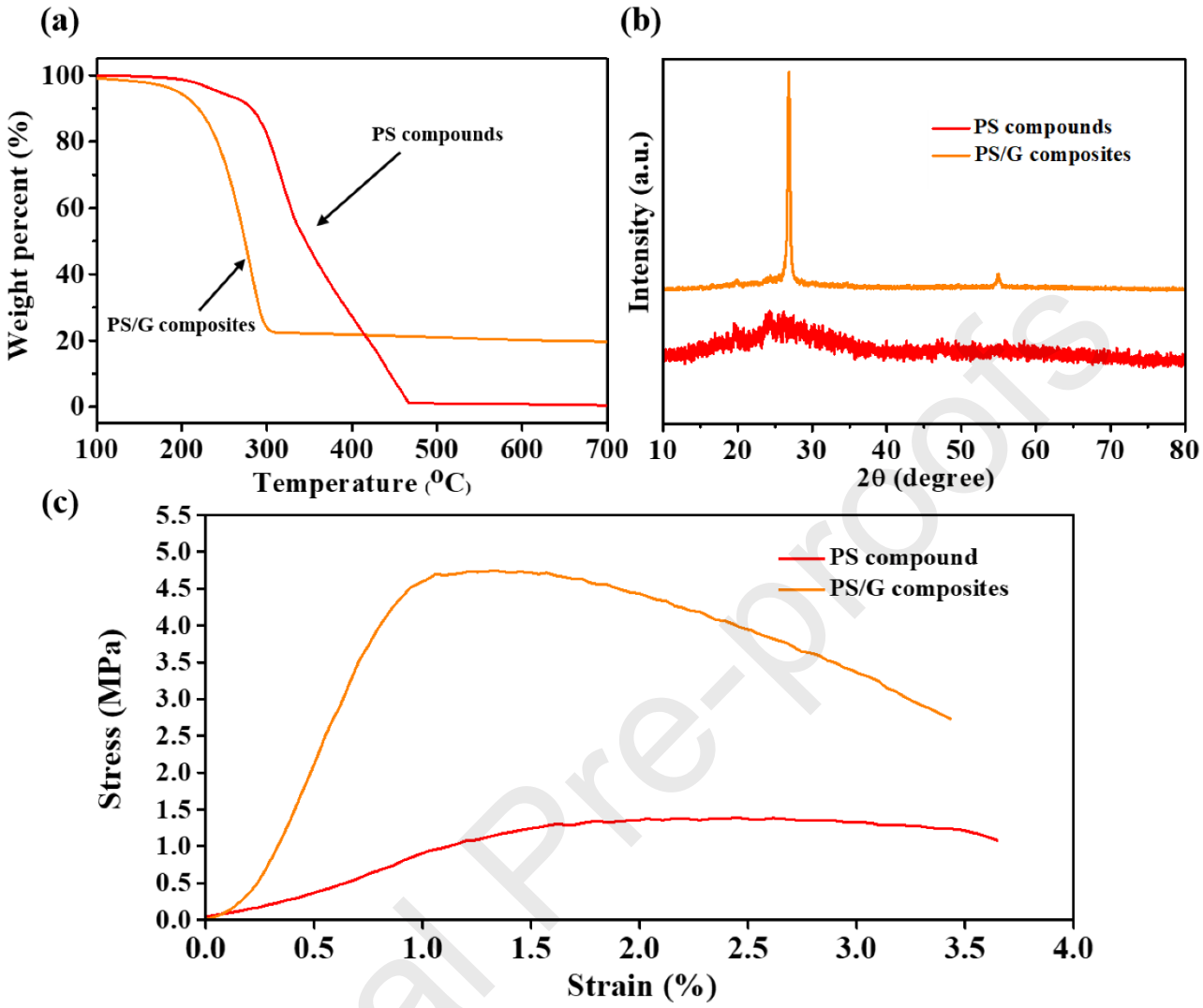


**Figure 3.** (a) TGA plot, (b) XRD patterns, and (c) Stress–strain curve of PS compounds and PS/G composites.

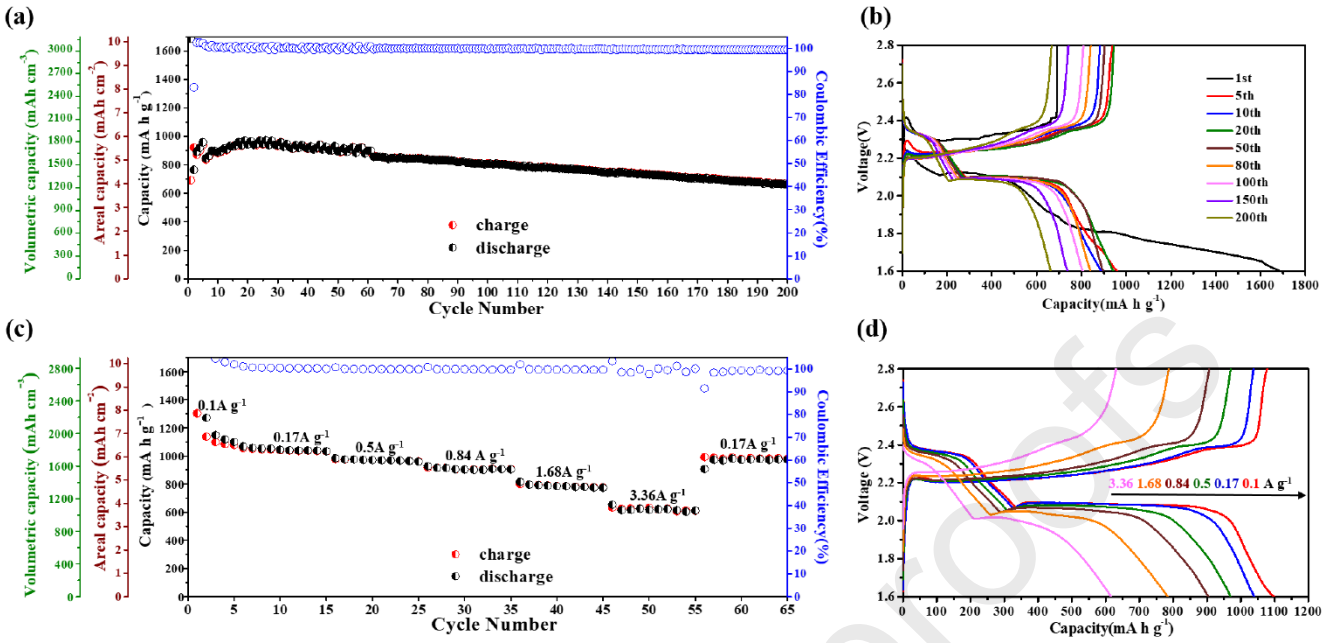


**Figure 4.** (a) Cycling performance of PS/G composites at a rate of 0.17 A g-1 (first five cycles are 0.1 A $g^{-1}$). (b) Voltage profiles of PS/G composites at a rate of 0.17 A g-1 (first five cycles are 0.1 A $g^{-1}$) between 1.6 and 2.8 V corresponding to (a). (c) The rate performance of PS/G composites electrode at various rates from 0.1 to 3.36 A $g^{-1}$. (d) Voltage profiles of PS/G composites at various rates from 0.1 to 3.36 A $g^{-1}$ corresponding to (c).

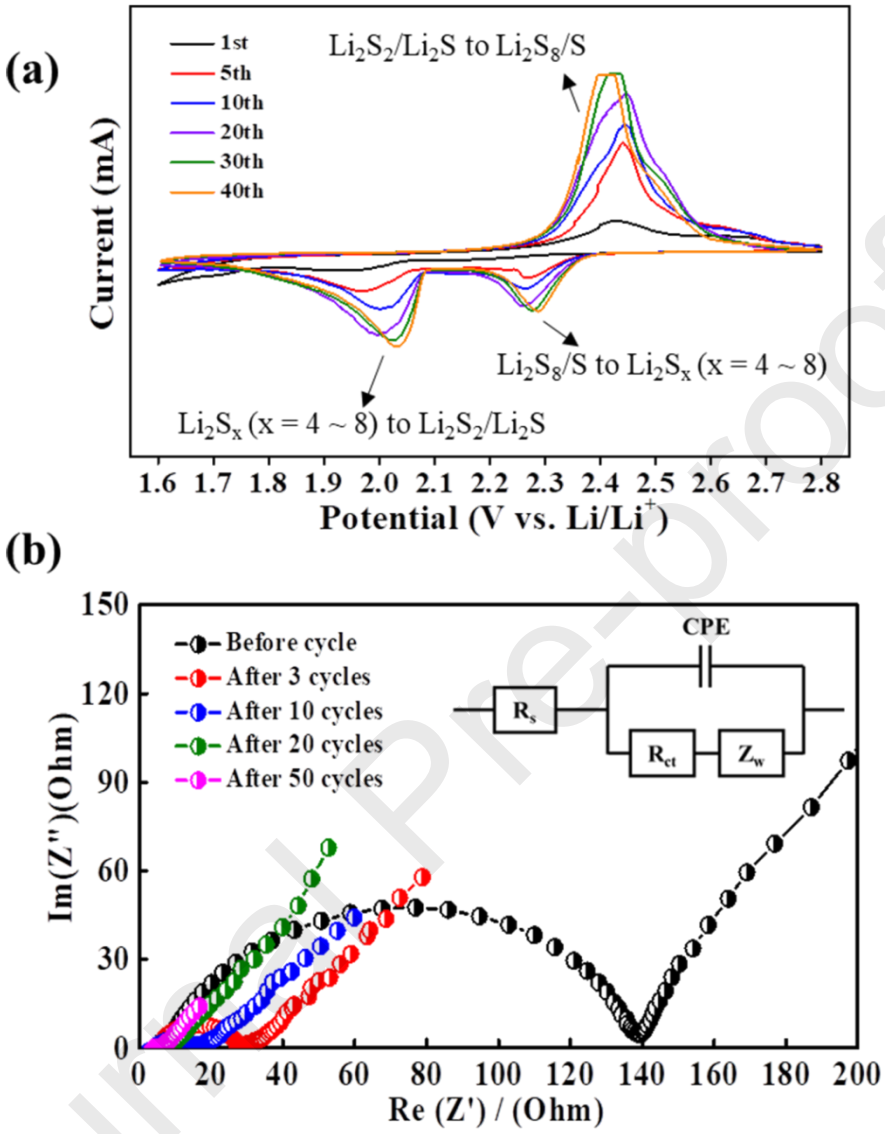


**Figure 5.** (a) cyclic voltammetry profiles of the PS/G composites at a scan rate of 0.1 mV $s^{-1}$. (b) EIS Nyquist plots of the PS/G composites before cycling to 50 cycles.

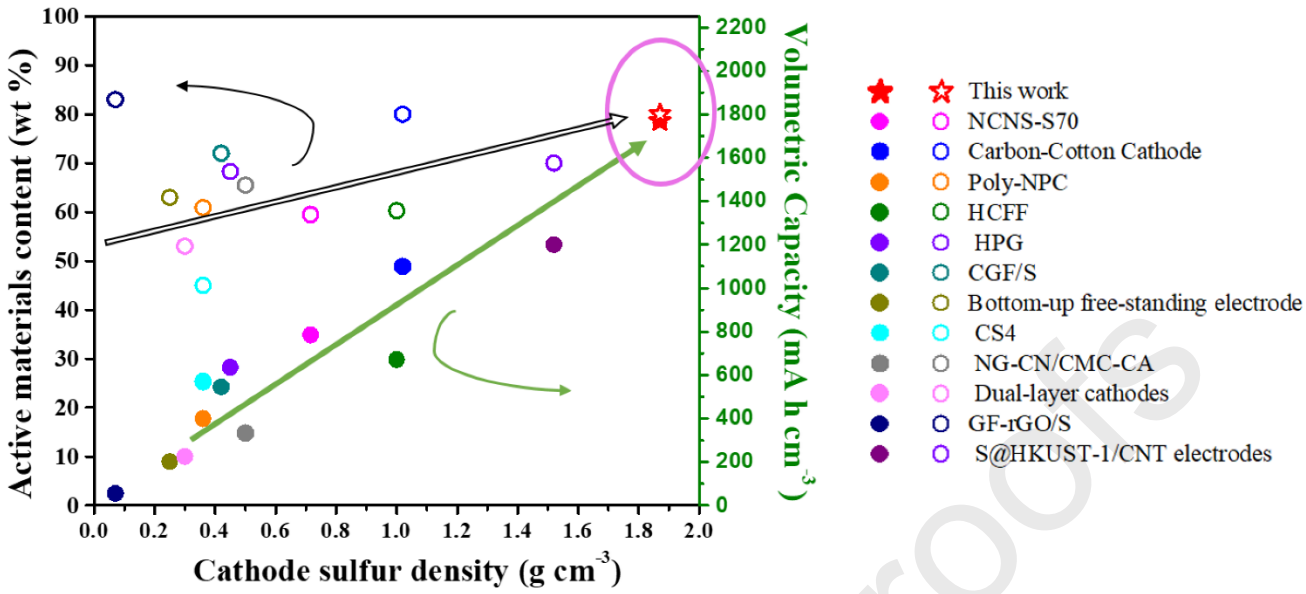


**Figure 6.** Comparison of the performance based on the PS/G composites cathode reported here and other recently published (reference circles): volumetric capacity (closed symbols) and sulfur content (open symbols) vs. cathode sulfur density.

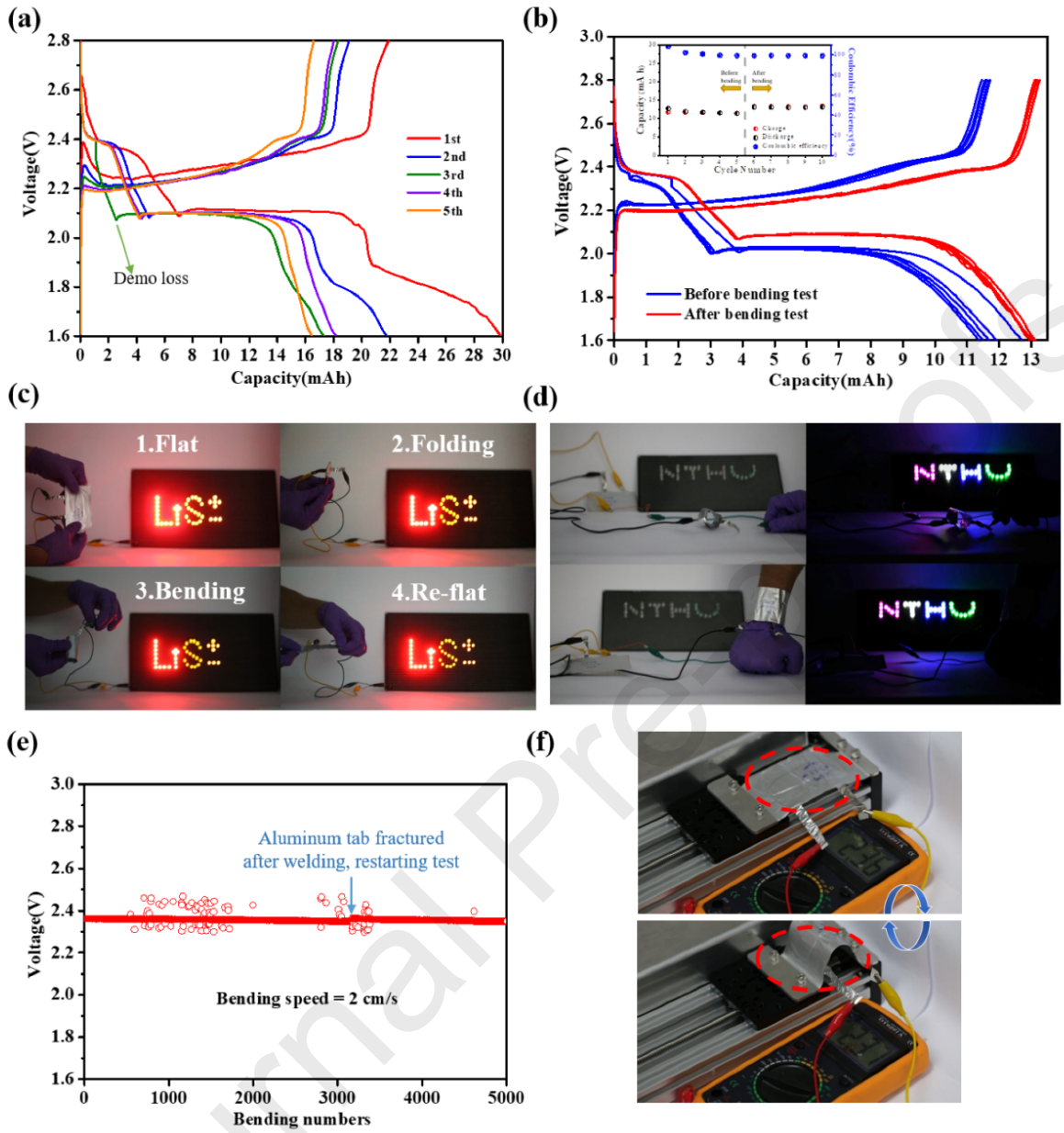


**Figure 7.** (a) The voltage profiles of the pouch cell at flat states of the first five cycles at a rate of 16.75 mA $g^{-1}$. (b) The voltage profiles of the pouch cell were at a rate of 167.5 mA $g^{-1}$ before and after bending, and the inset shows the cycling performance stability of pouch cell. (c) The photograph of pouch cell lights up an LED under different bending and folding angles. Movie S1 in the Supporting information shows the operation video. (d) The pouch-type battery in series at bending states lighted up 40 different

color LEDs. (e) Voltage retention during the fatigue test. (f) Demonstration of a cycle fatigue test: the flat (top) and bent (bottom) states of a flexible Li-S pouch cell. Movie S2 in the Supporting information shows the operation video.

**Supporting Information.** Experimental details of material preparation; details on material and electrochemical characterization; EDS spectra, $^{31}P$ NMR spectra and Raman shift of PS compounds and PS/G composites; electrochemical performance ($LiNO_3$ added DOL/DME electrolyte, LiTFSI electrolyte) of PS/G composites; images and voltage profiles of pouch cell in cylindrical bending state; detailed data of comparison of Li-S battery; movies (MPG) showing pouch cells light up an LED under different bending and folding angles, and the demonstration at a cycle fatigue test.

## AUTHOR INFORMATION

**Corresponding Author**

*hytuan@che.nthu.edu.tw (Hsing-Yu Tuan)

**ORCID :**

Hsing-Yu Tuan: 0000-0003-2819-2270

**Notes**

The authors declare no competing financial interest.

**ACKNOWLEDGMENT**

We acknowledge the financial support by the Ministry of Science and Technology through the grants of MOST 106- 2221-E-007-081-MY3, 106-2628-E-007-005-MY3, and 103- 2221-E-007-089-MY3, and MOST 106-2622-8-007-017, MOST 108-2636-E-007-013 and by National Tsing Hua University through the grant of 107Q2708E1.

## References

(1). Manthiram, A.; Fu, Y.; Su, Y.-S., *Acc. Chem. Res.* **2012,** *46*, 1125-1134.
(2). Yang, Y.; Zheng, G.; Cui, Y., *Chem. Soc. Rev.* **2013,** *42*, 3018-3032.
(3). Wild, M.; O'neill, L.; Zhang, T.; Purkayastha, R.; Minton, G.; Marinescu, M.; Offer, G., *Energy Environ. Sci.* **2015,** *8*, 3477-3494.
(4). Armand, M.; Tarascon, J.-M., *Nature* **2008,** *451*, 652.
(5). Cano, Z. P.; Banham, D.; Ye, S.; Hintennach, A.; Lu, J.; Fowler, M.; Chen, Z., *Nature Energy* **2018,** *3*, 279.
(6). Dunn, B.; Kamath, H.; Tarascon, J.-M., *Science* **2011,** *334*, 928-935.
(7). Seh, Z. W.; Sun, Y.; Zhang, Q.; Cui, Y., *Chem. Soc. Rev.* **2016,** *45*, 5605-5634.
(8). Barchasz, C.; Leprêtre, J.-C.; Patoux, S.; Alloin, F., *Electrochim. Acta* **2013,** *89*, 737-743.
(9). Yang, Y.; Zheng, G.; Cui, Y., *Energy Environ. Sci.* **2013,** *6*, 1552-1558.
(10). Yin, Y. X.; Xin, S.; Guo, Y. G.; Wan, L. J., *Angew. Chem. Int. Ed.* **2013,** *52*, 13186-13200.
(11). Ma, L.; Hendrickson, K. E.; Wei, S.; Archer, L. A., *Nano Today* **2015,** *10*, 315-338.
(12). Manthiram, A.; Fu, Y.; Chung, S.-H.; Zu, C.; Su, Y.-S., *Chem. Reviews* **2014,** *114*, 11751-11787.
(13). Schuster, J.; He, G.; Mandlmeier, B.; Yim, T.; Lee, K. T.; Bein, T.; Nazar, L. F., *Angew. Chem. Int. Ed.* **2012,** *51*, 3591-3595.
(14). Jayaprakash, N.; Shen, J.; Moganty, S. S.; Corona, A.; Archer, L. A., *Angew. Chem. Int. Ed.* **2011,** *50*, 5904-5908.
(15). Xiao, L.; Cao, Y.; Xiao, J.; Schwenzer, B.; Engelhard, M. H.; Saraf, L. V.; Nie, Z.; Exarhos, G. J.;

Liu, J., *Adv. Mater.* **2012,** *24*, 1176-1181.
(16).Chen, W.; Lei, T.; Lv, W.; Hu, Y.; Yan, Y.; Jiao, Y.; He, W.; Li, Z.; Yan, C.; Xiong, J., *Adv. Energy Mater.* **2018,** *30*, 1804084.
(17).Liu, B.; Bo, R.; Taheri, M.; Bernardo, I.-D.; Motta, N.; Chen, H.;Tsuzuki, T.; Yu, G.; Tricol, A., *Nano Lett.* **2019,** *19*, 4391-4399.
(18).Xiao, Z.; Yang, Z.; Li, Z.; Li, P.; Wang, R., *ACS. Nano* **2019,** *13*, 3404-3412.
(19).Zhou,L.; Yao, L.; Li, S.; Zai, J.; Li, S.; He, Q.;He, K.; Li, K.; Wang, D.; Qian, X., *J. Mater. Chem. A* **2019,** *7*, 3618.
(20).Zhang, Z.; Wu, D.-H.;Zhou, Z.; Li, G.-R.; Liu, S.;Gao, X.-P., *Sci China Mater* **2019,** *62(1)*, 74-86.
(21).Xiao, Z.; Li, Z.; Li, P.; Meng, X.; Wang, R., *ACS Nano* **2019,** *13*, 3608-3617.

(22).Xi, K.; He, D.; Harris, C.; Wang, Y.; Lai, C.; Li, H.; Coxon, P.-R.; Ding, S.; Wang, C.; Kumar, R.-V., *Adv. Sci.* **2019,** *6*, 1800815.
(23).Lei, T.; Chen, W.; Huang, J.; Yan, C.; Sun, H.; Wang, C.; Zhang, W.; Li, Y.; Xiong, J., *Adv. Energy Mater.* **2017,** *7*, 1601843.
(24). Tang, C.; Zhang, Q.; Zhao, M. Q.; Huang, J. Q.; Cheng, X. B.; Tian, G. L.; Peng, H. J.; Wei, F., *Adv. Mater.* **2014,** *26*, 6100-6105.
(25). Song, J.; Gordin, M. L.; Xu, T.; Chen, S.; Yu, Z.; Sohn, H.; Lu, J.; Ren, Y.; Duan, Y.; Wang, D., *Angew. Chem. Int. Ed.* **2015,** *127*, 4399-4403.
(26). Qiu, Y.; Li, W.; Zhao, W.; Li, G.; Hou, Y.; Liu, M.; Zhou, L.; Ye, F.; Li, H.; Wei, Z., *Nano Lett.* **2014,** *14*, 4821-4827.
(27). Song, J.; Yu, Z.; Gordin, M. L.; Wang, D., *Nano Lett.* **2016,** *16*, 864-870.
(28). Wang, Z.; Dong, Y.; Li, H.; Zhao, Z.; Wu, H. B.; Hao, C.; Liu, S.; Qiu, J.; Lou, X. W. D., *Nature communications* **2014,** *5*, 5002.
(29).Wang, Z.-U.;Wang, L.;Liu, S.; Li, G.-R.; Gao, X.-P., *Adv. Funct. Mater.* **2019,** *29*, 1901051.
(30).Li, H.; Tao, Y.; Zhang, C., Liu, D.; Luo, J.; Fan, W.; Xu, Y.; Li, Y.; You, C.; Pan, Z.-Z.; Ye, M.; Chen, Z.; Dong, Z.; Wang, D.-W.; Kang, F.; Lu, J.; Yang, Q.-H., *Adv. Energy Mater.* **2018**, 1703438.
(31). Balach, J.; Jaumann, T.; Klose, M.; Oswald, S.; Eckert, J. r.; Giebeler, L., *J. Phys. Chem. C* **2015,** *119*, 4580-4587.
(32). Kong, W.; Yan, L.; Luo, Y.; Wang, D.; Jiang, K.; Li, Q.; Fan, S.; Wang, J., *Adv. Funct. Mater.* **2017,** *27*, 1606663.
(33).Shia, H.; Zhaoa, X.; Wua, Z.-S.; Donga, Y.; Lua, P.;Chena, J.; Rend, W.; Chengd, H.-M.; Bao, X., *Nano Energy* **2019,** *60*, 743-751.
(34).Lei, T.; Chen, W.; Lv, W.; Huang, J.; Zhu, J. et al., *Joule* **2018,** *2*, 2091-2104.
(35).Lei, T.; Chen, W.; Hu, Y.; Lv, W.;Lv, X.;Yan, Y.; Huang, J.; Jiao, Y.; Chu, J.; Yan, C.; Wu, C.;Li, Q.; He, W.; Xiong, J., *Adv. Mater.* **2018,** *8*, 1802441.
(36).Chen, W.;Lei, T.;Wu, C.; Deng, M.;Gong, C.;Hu, K.;Ma, Y.;Dai, L.; Lv, W.;He, W.;Liu, X.; Xiong,

J.; Yan, C., *Adv. Mater.* **2018,** *8*, 1702348.
(37). Lv, D.; Zheng, J.; Li, Q.; Xie, X.; Ferrara, S.; Nie, Z.; Mehdi, L. B.; Browning, N. D.; Zhang, J. G.; Graff, G. L., *Adv. Energy Mater.* **2015,** *5*, 1402290.
(38). Hagen, M.; Hanselmann, D.; Ahlbrecht, K.; Maça, R.; Gerber, D.; Tübke, J., *Adv. Energy Mater.* **2015,** *5*, 1401986.
(39). Chung, S.-H.; Chang, C.-H.; Manthiram, A., *Energy Environ. Sci.* **2016,** *9*, 3188-3200.
(40). Chung, S.-H.; Chang, C.-H.; Manthiram, A., *ACS Nano* **2016,** *10*, 10462-10470.
(41). Yuan, Z.; Peng, H. J.; Huang, J. Q.; Liu, X. Y.; Wang, D. W.; Cheng, X. B.; Zhang, Q., *Adv. Funct. Mater.* **2014,** *24*, 6105-6112.
(42). Fang, R.; Zhao, S.; Hou, P.; Cheng, M.; Wang, S.; Cheng, H. M.; Liu, C.; Li, F., *Adv. Mater.* **2016,** *28*, 3374-3382.
(43). Peng, H. J.; Xu, W. T.; Zhu, L.; Wang, D. W.; Huang, J. Q.; Cheng, X. B.; Yuan, Z.; Wei, F.; Zhang, Q., *Adv. Funct. Mater.* **2016,** *26*, 6351-6358.
(44). Hu, G.; Xu, C.; Sun, Z.; Wang, S.; Cheng, H. M.; Li, F.; Ren, W., *Adv. Mater.* **2016,** *28*, 1603-1609.
(45). Xiao, P.; Bu, F.; Yang, G.; Zhang, Y.; Xu, Y., *Adv. Mater.* **2017,** *29*, 1703324.
(46). Pei, F.; Lin, L.; Ou, D.; Zheng, Z.; Mo, S.; Fang, X.; Zheng, N., *Nature Commun.* **2017,** *8*, 482.
(47). Ozturk, T.; Ertas, E.; Mert, O., *Chemical reviews* **2010,** *110*, 3419-3478.
(48). Andrews, L.; Reynolds, G. G.; Mielke, Z.; McCluskey, M., *Inor. Chem.* **1990,** *29*, 5222-5225.
(49). Chung, W. J.; Griebel, J. J.; Kim, E. T.; Yoon, H.; Simmonds, A. G.; Ji, H. J.; Dirlam, P. T.; Glass, R. S.; Wie, J. J.; Nguyen, N. A., *Nature Chem.* **2013,** *5*, 518.
(50). Li, X.; Liang, J.; Lu, Y.; Hou, Z.; Cheng, Q.; Zhu, Y.; Qian, Y., *Angew. Chem. Int. Ed.* **2017,** *56*, 2937-2941.
(51). Quan, Z.; Hirayama, M.; Sato, D.; Zheng, Y.; Yano, T. a.; Hara, K.; Suzuki, K.; Hara, M.; Kanno, R., *J. Amer. Ceram. Soc.* **2017,** *100*, 746-753.
(52). Song, J.; Yu, Z.; Gordin, M. L.; Hu, S.; Yi, R.; Tang, D.; Walter, T.; Regula, M.; Choi, D.; Li, X., *Nano Lett.* **2014,** *14*, 6329-6335.
(53). Wang, Y.; Sherwood, P. M., *Surf. Sci. Spectra* **2002,** *9*, 159-165.
(54). Quan, B.; Yu, S.-H.; Chung, D. Y.; Jin, A.; Park, J. H.; Sung, Y.-E.; Piao, Y., *Sci. Rep.* **2014,** *4*, 5639.
(55). Raccichini, R.; Varzi, A.; Passerini, S.; Scrosati, B., *Nature Mater.* **2015,** *14*, 271.
(56). Hou, T.-Z.; Xu, W.-T.; Chen, X.; Peng, H.-J.; Huang, J.-Q.; Zhang, Q., *Angew. Chem. Int. Ed.* **2017**, *56*, 8178-8182.
(57). Maihom, T.; Kaewruang, S.; Phattharasupakun, N.; Chiochan, P.; Limtrakul, J.; Sawangphruk, M., *J. Phys. Chem. C* **2018**, *122*, 7033-7040.
(58). Kong, L.; Chen, X.; Li, B.-Q.; Peng, H.-J.; Huang, J.-Q.; Xie, J.; Zhang, Q., *Adv. Mater.* **2018**, *30*, 1705219.
(59). Jensen, J.; Zeroka, D.; Banerjee, A., *J. Mol. Struct.* **2000,** *505*, 31-43.

(60). Lin, Z.; Liu, Z.; Fu, W.; Dudney, N. J.; Liang, C., *Angew. Chem. Int. Ed.* **2013,** *125*, 7608-7611.
(61). Jensen, J.; Zeroka, D., *J. Mol. Struct.* **1999,** *487*, 267-274.
(62). Chu, H.-C.; Chang, Y.-C.; Lin, Y.; Chang, S.-H.; Chang, W.-C.; Li, G.-A.; Tuan, H.-Y., *ACS Appl. Mater. Interfaces* **2016,** *8*, 13009-13017.
(63). Huang, J.-Q.; Zhuang, T.-Z.; Zhang, Q.; Peng, H.-J.; Chen, C.-M.; Wei, F., *ACS Nano* **2015,** *9*, 3002-3011.
(64). Chung, S. H.; Han, P.; Singhal, R.; Kalra, V.; Manthiram, A., *Adv. Ener. Mater.* **2015,** *5*, 1500738.
(65). Deng, Z.; Zhang, Z.; Lai, Y.; Liu, J.; Li, J.; Liu, Y., *J. Electrochem. Soc.* **2013,** *160*, A553-A558.
(66). Hu, C.; Kirk, C.; Cai, Q.; Cuadrado-Collados, C.; Silvestre-Albero, J.; Rodríguez-Reinoso, F.; Biggs, M. J., *Adv. Ener. Mater.* **2017,** *7*, 1701082.
(67). Li, M.; Zhang, Y.; Hassan, F.; Ahn, W.; Wang, X.; Liu, W. W.; Jiang, G.; Chen, Z., *J. Mater. Chem.* **2017,** *5*, 21435-21441.
(68). Fang, R.; Zhao, S.; Pei, S.; Qian, X.; Hou, P.-X.; Cheng, H.-M.; Liu, C.; Li, F., *ACS Nano* **2016,** *10*, 8676-8682.
(69). Pang, Q.; Liang, X.; Kwok, C. Y.; Kulisch, J.; Nazar, L. F., *Adv. Energy Mater.* **2017,** *7*, 1601630.
(70). Qie, L.; Zu, C.; Manthiram, A., *Adv. Ener. Mater.* **2016,** *6*, 1502459.
(71). Mao, Y.; Li, G.; Guo, Y.; Li, Z.; Liang, C.; Peng, X.; Lin, Z., *Nature Commun.* **2017,** *8*, 14628.

Highlight:

- A phosphor-sulfur/graphene composite is demonstrated as a Li-S battery cathode.
- PS/G composites achieve a high volumetric capacity of 1726 mA h $cm^{-3}$.
- PS/G composites have a high sulfur loading of 6 ~ 10 mg $cm^{-2}$.
- A pouch cell exhibits stable performance under bending and folding.